Memory-functionality superconductor/ferromagnet/superconductor junctions based on the high-T_c cuprate superconductors YBa$_2$Cu$_3$O$_{7-x}$ and the colossal magnetoresistive manganite ferromagnets La$_{2/3}$X$_{1/3}$MnO$_{3+\delta}$ (X = Ca, Sr)

R. de Andrés Prada,[1,2] T. Golod,[1] O. M. Kapran,[1] E. A. Borodianskyi,[1] Ch. Bernhard,[2] and V. M. Krasnov[1,3,*]

[1]*Department of Physics, Stockholm University, AlbaNova University Center, SE-10691 Stockholm, Sweden*
[2]*Physics Department and Fribourg Center for Nanomaterials, University of Fribourg, Chemin du Musée 3, CH-1700 Fribourg, Switzerland*
[3]*Moscow Institute of Physics and Technology, State University, 9 Institutskiy pereulok, Dolgoprudny, Moscow Region 141700, Russia*

Complex oxides exhibit a variety of unusual physical properties, which can be used for designing novel electronic devices. Here we fabricate and study experimentally nanoscale superconductor/ferromagnet/ superconductor junctions with the high-T_c cuprate superconductors YBa$_2$Cu$_3$O$_{7-x}$ and the colossal magnetoresistive (CMR) manganite ferromagnets La$_{2/3}$X$_{1/3}$MnO$_{3+\delta}$ (X=Ca or Sr). We demonstrate that in a broad temperature range the magnetization of a manganite nanoparticle, forming the junction interface, switches abruptly in a monodomain manner. The CMR phenomenon translates the magnetization loop into a hysteretic magnetoresistance loop. The latter facilitates a memory functionality of such a junction with just a single CMR ferromagnetic layer. The orientation of the magnetization (stored information) can be read out by simply measuring the junction resistance in a finite magnetic field. The CMR facilitates a large readout signal in a small applied field. We argue that such a simple single-layer CMR junction can operate as a memory cell both in the superconducting state at cryogenic temperatures and in the normal state up to room temperature.

I. INTRODUCTION

The competition between the antagonistic phenomena of spin-singlet superconductivity and spin-polarized ferromagnetism in superconductor/ferromagnet (S/F) heterostructures leads to several unusual phenomena, which are interesting for both fundamental and applied research [1–5]. In particular, hybrid S/F structures are promising candidates for the creation of a scalable and dense cryogenic memory. Such memory is needed for a superconducting digital exaflop computer, which can significantly outperform a semiconducting analog in both speed and energy efficiency [6–8]. At present there is no suitable cryogenic random access memory (RAM) for the superconducting computer. This is considered to be the "main obstacle to the realization of high performance computer systems and signal processors based on superconducting electronics" [9]. Several new concepts for scalable, nanometer-sized superconducting RAM, involving hybrid S/F structures, were proposed recently [10–16]. The nonvolatile memory function in ferromagnets is naturally provided by the finite coercive field for the remagnetization of the ferromagnetic particle, and the information is stored in the orientation of the magnetization. The conventional (room-temperature) magnetic RAM [17,18] contains a multilayered spin-valve structure, in which the information is stored in terms of the relative orientation of the magnetization of the F layers and the readout signal is provided by the orientation dependence of the resistance. In S/F memory cells the information is

also stored in the orientation, but the readout parameter is the critical superconducting current of the device.

One of the unusual phenomena in S/F spin valves is the possibility to generate a spin-triplet superconducting order parameter in the F layers. This should occur in the noncollinear state of the S/F spin valve and should lead to an enhancement of the supercurrent through the spin valve [1–3,19–24]. It is anticipated that this phenomenon should be most spectacular in a fully spin polarized ferromagnet, which would not be able to accommodate spin-singlet Cooper pairs [25–32]. The full spin polarization occurs naturally in half-metallic ferromagnets such as the manganite perovskite oxides considered in this work.

Perovskite oxides and related oxides with strongly correlated electrons are known for their complex phase diagrams, with coexisting and often competing interactions and orders that give rise to a wealth of unconventional states with outstanding properties [33–35]. The most prominent examples are the high-temperature superconductivity (HTSC) [36] in the cuprates and the colossal magnetoresistance (CMR) in the manganites [37], but there is also a wide range of ferro- and antiferromagnetic, ferroelectric, multiferroic, charge/spin density wave, and orbital ordered states. Their versatile physical properties can be readily tuned by chemical substitution, which affects the carrier concentration and/or the crystal structure, external pressure, stress, temperature, and electric [38] and magnetic fields. Such a tunability is very interesting for fundamental research of unconventional states of matter as well as for designing novel electronic devices with new functionality. However, the sensitivity of the perovskites to structural modifications also requires accurate control of the

*Vladimir.Krasnov@fysik.su.se

thin-film structure and the crystalline and chemical quality. In recent years it has been demonstrated that such control can be achieved via the heteroepitaxial growth of complex oxide multilayers with sequentially matching crystal structures [39–41]. Several all-perovskite electronic devices have already been demonstrated, such as solar cells [42,43], memristors, and resistive RAM [44].

Heteroepitaxial thin-film multilayers of the cuprate HTSC $YBa_2Cu_3O_{7-x}$ (YBCO) and the ferromagnetic manganites $La_{2/3}Ca_{1/3}MnO_{3+\delta}$ (LCMO) and $La_{2/3}Sr_{1/3}MnO_{3+\delta}$ (LSMO) can be readily grown, thanks to the good matching of their crystal structures [45–51]. High superconducting critical temperatures $T_c = 90$ K of YBCO and Curie temperature $T_{Curie} = 270/370$ K of LCMO/LSMO enable operation of S/F devices based on such heterostructures at the liquid-nitrogen temperature, which is advantageous for various potential future applications.

In this work we fabricate and study experimentally complex oxide YBCO/LCMO/YBCO and YBCO/LSMO/YBCO nanoscale junctions with a minimum feature size of $\sim$275 nm. We demonstrate that such SFS junctions with a single colossal magnetoresistive F layer can be used as memory cells. In such a S-CMR-S memory the information is stored in the orientation of the magnetization of the single F layer. However, in contrast to previous memory prototypes based on SFS Josephson junctions, the readout in our devices is based entirely on the CMR phenomenon measured across the junction and does not rely on the unconventional proximity effect and triplet superconductivity in the F interlayer. We demonstrate that the CMR effect allows us to reconstruct the magnetization loop of a single F nanoparticle that forms the junction barrier. The magnetization loops are characterized by an abrupt switching between saturated magnetization states, typical for a monodomain state of the ferromagnetic interlayer. Since YBCO is a high-temperature superconductor with $T_c \simeq 90$ K, our devices can operate comfortably at liquid-nitrogen temperatures. Furthermore, since we are not using the superconducting critical current for readout, such a device can operate above T_c and even at room temperature. Therefore, we conclude that such cuprate/manganate heterostructures can be used to create complex oxide electronic and spintronic devices that are both superconducting at cryogenic temperatures and normal conducting at room temperature.

II. EXPERIMENT

SFS trilayers composed of $YBa_2Cu_3O_7$ and LCMO or LSMO were grown by pulsed laser deposition on (001)-oriented $La_{0.3}Sr_{0.7}Al_{0.65}Ta_{0.35}O_3$ (LSAT) substrates (Crystec) using an excimer KrF laser ($\lambda = 248$ nm, $t_s = 25$ ns). The trilayer denoted as LC_10 has the structure YBCO (100 nm)/LCMO (10 nm)/YBCO (100 nm), while the one labeled LS_11 is YBCO (100 nm)/LSMO (11 nm)/YBCO (100 nm). They were grown at 840 °C in a partial pressure of 0.34 mbar of O_2 with a laser fluency of 1.42 J cm^{-2} and a frequency of 7 Hz. Subsequently, the samples were cooled to 700 °C, where the pressure was increased to 1 bar of pure O_2, and further cooled at a rate of to 30 °C per minute to a first *in situ* annealing step at 485 °C and a second one at

400 °C (each for 1 h) to ensure full oxygenation of the trilayer. Finally, the trilayers were coated with 100 nm of Au (using a thermal evaporator) as a protective layer during the device fabrication.

The dc magnetization was measured with the vibrating sample magnetometer (VSM) of a physical properties measurement system by Quantum Design. The magnetic field was applied parallel to the film surface. The magnetic signal from the LSAT substrate was subtracted to obtain the magnetization of the film, which in the presentation below is scaled to a magnetic moment per Mn atom. Below the superconducting transition of YBCO the interpretation of the VSM data is complicated by the diamagnetic signal of YBCO. Therefore, we show in the following only the data above 90 K.

The SFS junctions were made from the trilayers using nanofabrication techniques. First, fingerlike electrodes of $\sim$6 μm in width were defined on the samples by optical lithography and cryogenic reactive ion etching at −50 °C in Ar plasma. Cryogenic etching preserves the oxygen content in the oxides and minimizes the deterioration of the samples. Next, the samples were transferred to a dual-beam scanning electron microscope (SEM)–Ga$^+$ focused ion beam (FIB) system. Using the FIB, we made narrow bridges in the electrodes of $\sim$2 μm in length and $\sim$275 nm in width. Subsequently, the sample was tilted to a glazing angle with respect to the FIB column, and two side cuts were made to interrupt the bottom and top YBCO layers in the bridge, forcing the current flow through the F barrier. Details of the fabrication procedure can be found in Ref. [31].

Figures 1(a) and 1(b) show SEM images of junctions on samples LC_10 and LS_11, respectively. In Fig. 1(a) the interrupting cuts are $\sim$700 nm apart, thus creating an $\sim$700 × 275 nm^2 LCMO junction. For LS_11 in Fig. 1(b), the LSMO junction is $\sim$560 × 275 nm^2. A sketch of the junctions that consist of a single F layer sandwiched between two S electrodes is displayed in Fig. 1(c). The electric current through the bridge is interrupted by the side cuts, forcing it to flow in the vertical direction through the F layer. The current path is shown by the red arrows.

Transport measurements were performed in a closed-cycle ^{4}He cryostat with the samples cooled in He gas. The cryostat is equipped with a superconducting magnet for magnetic fields up to 17 T. The samples were mounted on a rotating sample holder that enables measurements in different field configurations. The in-plane and out-of-plane orientations considered below are indicated in Fig. 1(c). The junctions are contacted by bonding four electrodes to the top Au layer. Two independent voltage and current contacts on each side of the bridge facilitate four-probe measurements. At $T < T_c$ they allow us to directly probe the junction characteristics, whereas above T_c the bridge resistance adds to the measured signal.

Figures 1(d) and 1(e) display the dc magnetization data of the unpatterned trilayer films (before the junctions were fabricated). Figure 1(d) shows the temperature-dependent magnetization $M(T)$ of both samples, during cooling with an in-plane-oriented field of $H = 1000$ Oe. The onset of the ferromagnetic signal occurs for the LCMO layer of the LC_10 sample at $T_{Curie} \sim 210$ K and for the LSMO layer of LS_11 already above 300 K, roughly consistent with $T_{Curie} \sim 270$ and 370 K reported for bulk LCMO and LSMO crystals, respectively

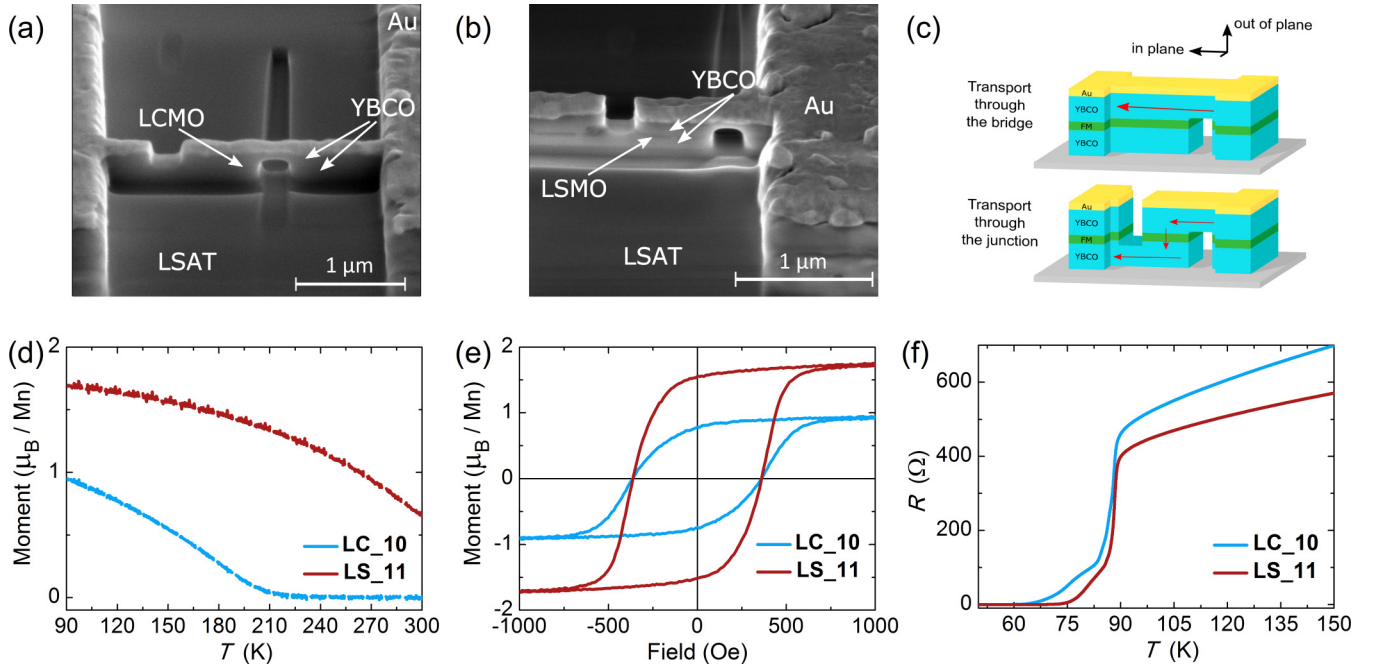FIG. 1. (a) SEM image of a YBCO/LCMO/YBCO junction on the LC_10 sample. (b) SEM image of a YBCO/LSMO/YBCO junction on LS_11. (c) Sketches of a bridge (top) and a junction (bottom) nanosculptured by focused Ion Beam from SFS trilayers (not in scale). Red arrows indicate the current flow path through the structures. Black arrows indicate field orientations. (d) The dc magnetization versus temperature obtained from the unpatterned trilayers while cooling in 1000 Oe applied in plane. (e) $M(H)$ hysteresis loops for the same films at 100 K (field in plane). (f) $R(T)$ showing the superconducting transition of the YBCO electrodes, obtained from patterned bridges on LC_10 and LS_11, respectively. The resistances are measured by applying a small ac current of 0.3 μA for LC_10 and 1 μA for LS_11.

[52,53]. The magnetic moment per Mn reaches values of 0.95 μ_B for LCMO and 1.7 μ_B for LSMO at $T = 90$ K. These values are considerably lower than in the corresponding bulk materials (with a low-T saturation moment of about 3.7 μ_B [52,53]) but are still characteristic of a pronounced ferromagnetic response of these very thin manganite layers. Figure 1(e) displays the magnetization versus field $M(H)$ loops for both samples at $T = 100$ K. A clear hysteretic behavior is observed for both samples with very similar coercive fields of $H_{Coer} \sim$ 360 Oe. Overall, the presented VSM data confirm that the thin manganite layers of these heterostructures exhibit a sizable ferromagnetic response.

Figure 1(f) compares the temperature dependence of the resistance $R(T)$ of the YBCO layers of both trilayers. These results were obtained from nanobridges at which only one of the two side cuts was made. Consequently, the bias current does not cross the manganite layer but flows along one of the YBCO electrodes. The plots thus represent the electronic response and superconducting transition of YBCO alone. The $R(T)$ curves are metallic in the normal state and exhibit clear superconducting transitions with an onset at $T_c \sim 90$ K. This proves that the superconducting state of the YBCO layers is preserved during the nanofabrication [54].

III. RESULTS AND DISCUSSION

Figure 2 summarizes the R vs T measurements and the current-voltage characteristics (I-V) at the base temperature of 7 K in different magnetic fields, obtained from the junctions made on the LC_10 and LS_11 trilayers. Figure 2(a) shows

representative $R(T)$ curves as measured with a small ac-bias current of $I_{ac} = 0.1$ μA for a junction on LC_10 at zero field (black line) and at 10 T for in-plane (red line) and out-of-plane (blue line) orientations. A SEM picture of this junction is shown in Fig. 1(a).

It is evident that the junction has a much higher resistance than the bridge [see Fig. 1(f)] and displays an insulating T dependence. Furthermore, it exhibits a large negative magnetoresistance (MR), characteristic of the CMR effect in manganites. The CMR appears below $T_{Curie} \simeq 210$ K, increases rapidly below $\sim$150 K, and is almost isotropic with respect to the field orientation. These data suggest that the thin LCMO layer behaves as a ferromagnetic insulator (FI) with a small band gap, qualitatively similar to the LaMnO$_{3+\delta}$ (LMO) layers of the previously studied junctions of Refs. [31,55]. From Fig. 2(a) it can also be seen that the low-bias $R(T)$ does not drop at T_c and continues to increase with decreasing temperature. Therefore, at this low bias, there is no supercurrent passing through the 10-nm-thick FI layer. This indicates that the LCMO layer is uniform (without microshots) and that there is no direct tunneling of Cooper pairs through the LCMO barrier.

Figure 2(b) shows $R(T)$ for the same junction measured at a 500 times larger ac current of $I_{ac} = 50$ μA. At this high bias signatures of the superconducting transition are clearly seen, although the resistance does not drop to zero. Figure 2(c) shows a similar behavior for the junction with the LSMO barrier measured at an intermediate current of $I_{ac} = 1$ μA. This type of unusual superconducting proximity effect through a FI layer at large bias was reported earlier for
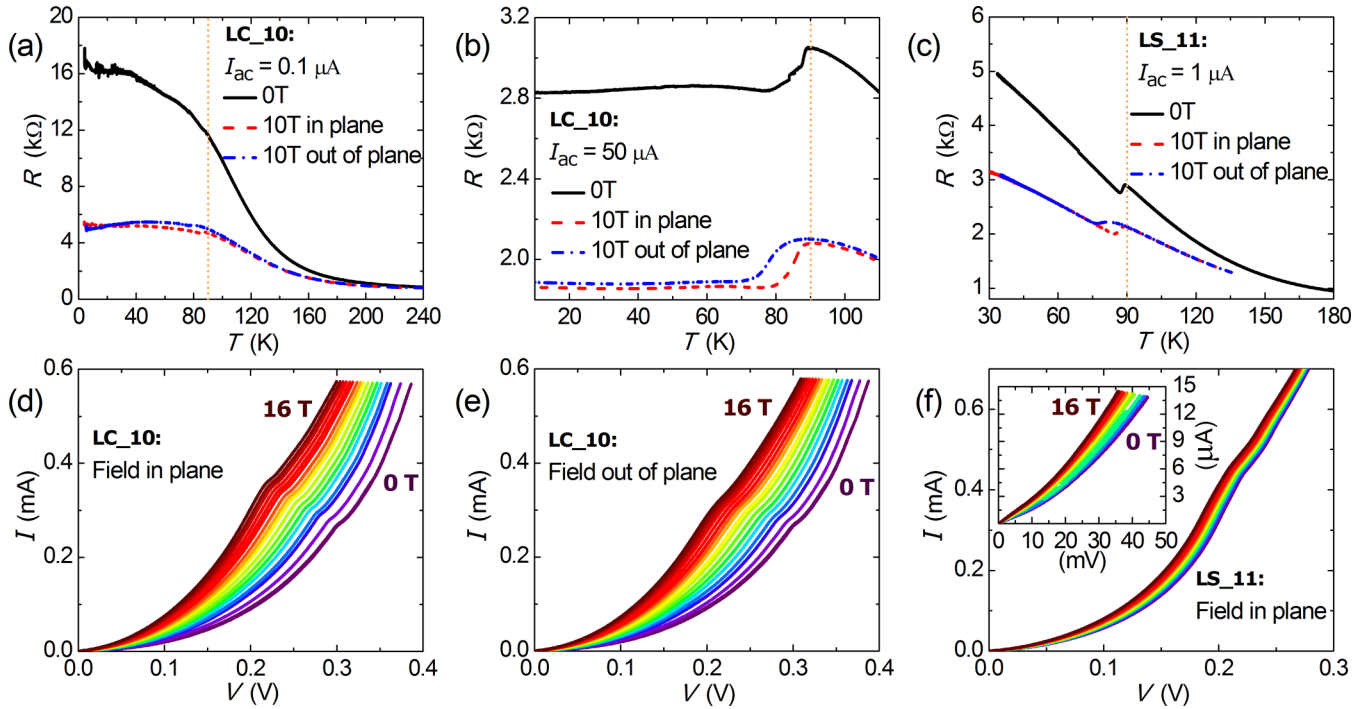
FIG. 2. (a)–(c) R vs T curves of the SFS junctions, obtained while cooling in different magnetic fields with applied ac currents of (a) 0.1 μA and (b) 50 μA on a junction on LC_10 and (c) 1 μA on a junction on LS_11. The dotted vertical lines indicate T_c for YBCO in zero field. (d) and (e) Field dependence of the I-V curves at $T = 7$ K on the same LC_10 junction with the field oriented (d) in plane and (e) out of plane. (f) In-plane field dependence of the I-V curves for LS_11 at 7 K. Inset: close-up of the low-bias parts of I-V. I-V are measured in a field ranging from 0 to 16 T with an increment of 1 T.

YBCO/LMO/YBCO junctions [31,55]. It was attributed to the occurrence of a Zener-type tunneling at a bias voltage larger than the band gap of the FI and subsequent direct Cooper pair transport in the conduction band of the FI.

Figures 2(d)–2(f) display I-V curves measured in the superconducting state at $T = 7$ K at different magnetic fields, ranging from 0 to 16 T with field increments of 1 T. Figures 2(d) and 2(e) show the data for the junction on LC_10 with in-plane and out-of-plane fields, respectively, and Fig. 2(f) shows the data for the junction on LS_11 with in-plane fields. The reduction of the resistance with increasing field, due to the negative CMR, is once more clearly seen. Note that, in line with the above-described bias dependence of the resistance, the I-V curves are strongly nonlinear with a decrease in the differential resistance towards increasing bias. There is also a well-defined kink in the I-V curves which in zero magnetic field occurs at $\simeq 0.3$ V for LCMO and $\simeq 0.2$ V for LSMO. Such a kink was also observed for the YBCO/LMO/YBCO junctions in Ref. [31] and explained in terms of Zener tunneling, leading to an anomalous high-bias proximity effect through the conduction band of the ferromagnetic insulator. Notably, the kink voltage in the I-V of the junctions with the LCMO and LSMO barriers [see Figs. 2(d)–2(f)] has a 4–5 times smaller value than for the junctions with the LMO barrier [31,55]. This trend is qualitatively consistent with the expectation that the band gaps of LCMO and LSMO, which should both be very close to a half-metallic state, are considerably smaller than the one of the ferromagnetic insulator LMO. Note that the weak insulatorlike behavior of the LCMO and LSMO layers (which in the bulk are half

metallic) can be understood in terms of the strain and disorder effects, which are common for such thin layers as well as a charge transfer at the interface between the manganite and YBCO [47,56,57].

Figure 3 shows the MR curves for a junction on LC_10 at different temperatures for an in-plane magnetic field. Figures 3(a)–3(c) show the MR curves for a small ac current of $I_{ac} = 0.1 \mu$A over a large field ranging from -10 to $+10$ T at representative temperatures of $T = 260$ K $> T_{Curie}$, $T_{Curie} > T = 100$ K $> T_c$, and $T = 10$ K $< T_c$, respectively. A negative MR, typical for the CMR manganites, occurs in the entire temperature range. Above $T_{Curie} \sim 210$ K of the LCMO layer [see Fig. 3(a)], the MR is relatively small, and the $R(H)$ curve has a smooth shape with a broad maximum at zero field that does not exhibit any hysteresis with respect to the direction of the field sweeping. Below T_{Curie} the CMR effect becomes rather large, with a maximal value of $\sim 200\%$ at 10 T at low T. As shown in the inset of Fig. 3(b), the $R(H)$ curves exhibit now clear hysteretic effects around the origin that are indicative of a field-induced magnetization switching of ferromagnetic nanoparticles, forming the junction interface, at a finite coercive field H_{Coer}.

Below T_c additional hysteresis effects and irregularities that appear in the MR curves [see Fig. 3(c)] are most likely related to Abrikosov vortices that enter the superconducting YBCO electrodes. The stray fields from these vortices can lead to large offset fields in the FM barrier (on the order of kilo-oersteds per vortex [15]). The vortex pinning thus can strongly affect the hysteresis and the shape of the measured MR curves. These vortex-induced effects can be avoided if
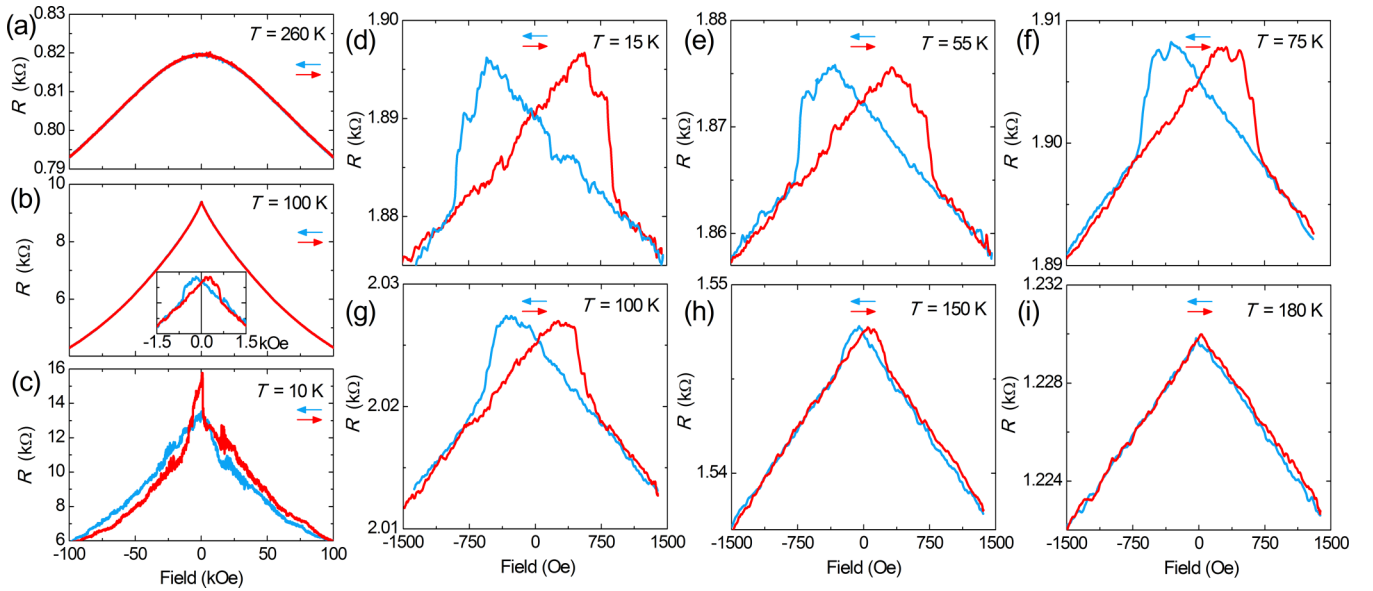
FIG. 3. Magnetoresistance (MR) curves of a junction on the LC_10 sample. (a)–(c) High-field MR curves measured with a low ac current of 0.1 μA at (a) $T > T_{Curie}$, (b) $T_{Curie} > T > T_c$, and (c) $T < T_c$. (d)–(i) MR curves in a small field range at different temperatures, measured with a higher ac current of 100 μA. Arrows indicate the direction of the field sweep. All fields are in plane oriented. The appearance of hysteretic MR loops is clearly seen, with an abrupt switching due to the remagnetization of the manganite interlayer.

the sweep range is limited to small enough fields for which the vortex cannot enter the sample. An estimate of this vortex entrance field can be obtained by dividing the flux quantum by the cross-sectional area of the electrode, which for our junctions is ~1 kOe due to the small cross-sectional area ($\simeq 100 \times 300$ nm^2) for the in-plane field orientation [see Fig. 1(c)]. The vortex entrance field is further increased by the mesoscopic nature of our junctions with an electrode size that is comparable to the London penetration depth of YBCO of $\lambda_{ab} \sim 200$ nm. Moreover, the metastability of the vortex state can be reduced by applying a larger transport current.

Figures 3(d)–3(i) show MR curves at different temperatures in a narrower field range measured with a larger ac current of 100 μA. The hysteresis between the MR curve for upward (red) and downward (blue lines) field sweeps is now evident, and the $R(H)$ curves are regular and very reproducible even below T_c. All the MR loops exhibit a qualitatively similar behavior. Upon decreasing the field, when going from the positive to negative field, $R(H)$ increases linearly up to a maximum at a small negative field at which the resistance decreases abruptly and in the following decreases linearly with the same absolute value of the slope as on the positive side. This hysteresis is most pronounced at low temperature, and its magnitude decreases continuously with increasing temperature without a clear disruption at T_c. This behavior is qualitatively different from the magnetoresistance of superconducting films induced by stray fields from ferromagnets in S/F hybrid films [58]. Therefore, the observed hysteresis on the MR loops is not related to vortices or superconductivity in YBCO but is solely associated with the CMR of LCMO and reflects the switching of magnetization in the F layer. This is fully consistent with our earlier conclusion that the resistance of the junction is almost entirely determined by the highly resistive manganite interlayer in the ferromagnetic

insulator state [see Figs. 1(f) and 2(a)]. The observation of such magnetoresistive hysteresis loops in junctions with a single manganite layer is our central result.

The above-described hysteresis of the MR curves has a fairly straightforward interpretation. The MR of the manganites depends on the absolute value of the magnetic induction $R(|B|)$, where $B = H + 4\pi M$ and M is the magnetization of the manganite layer. At high fields the ferromagnetic manganite layer is fully magnetized, and M reaches the saturation value M_s. Upon decreasing the applied field H (from positive to negative values), $R(|B|)$ increases due to the CMR effect for which $dR/d|B| < 0$. The $R(H)$ curve exhibits a constant linear slope as long as the manganite layer remains fully saturated. This changes only close to the negative coercive field $-H_{Coer}$ at which the magnetization flips to $-M_s$. Such a magnetization flipping causes a coaligned orientation of M and H which leads to an increase of the magnetic induction and a corresponding decrease of $R(B)$. The abrupt decrease of $R(B)$ at the corrective field thus reflects a sudden flipping of the magnetization of the ferromagnetic manganite layer. In general, the type of switching depends on the size and geometry of the F nanoparticle. We observe in most cases a somewhat abrupt change of $R(B)$ around H_{Coer} that is typical for the switching of a barrier with a single-domain ferromagnetic state along the easy axis of magnetization [the field parallel to the long side of an elongated F nanoparticle, as in our experiment; see Fig. 1(c)].

Figure 4 shows MR loops recorded from a junction on the YBCO/LSMO/YBCO trilayer. Figures 4(a) and 4(b) show $R(H)$ curves in a large field range of ± 10 T, measured at $I_{ac} = 1\,\mu$A at temperatures above and below T_c, respectively. A linear negative MR due to CMR in the LSMO layer is evident in Fig. 4(a). However, below T_c we also observe a jump in the resistance around 3 T. This jump disappears as the measurement current is increased (not shown). Figures 4(c)–
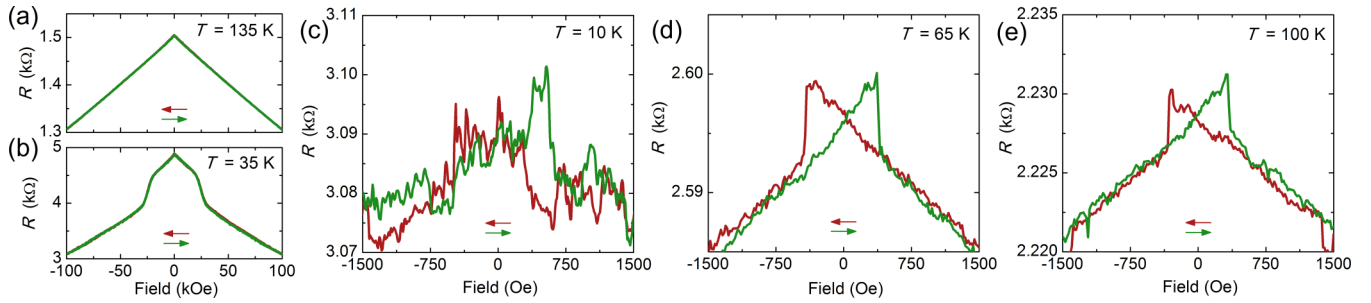
FIG. 4. MR of a junction on the YBCO/LSMO/YBCO sample. (a) and (b) High-field MR curves, measured with 1-μA ac bias at (a) $T_{\text{Curie}} > T > T_c$ and (b) $T < T_c$. (c)–(e) MR curves in a small field range at different temperatures, measured with 14-μA ac current. Arrows indicate the direction of the field sweeping. Fields are in plane oriented. The abrupt $R(H)$ switching indicates a monodomain magnetic configuration of the manganite nanoparticle.

4(e) display corresponding MR loops in a narrow field range, measured at a larger current of $I_{ac} = 14\,\mu$A, for the same junction. The overall hysteretic behavior is similar to that for the junction with the LCMO barrier in Fig. 3. At low T [Fig. 4(c)], we also see instabilities due to Abrikosov vortices, as in Fig. 3 (c). A closer comparison of the MR loops obtained from the junctions on LCMO and LSMO (Figs. 3 and 4) shows that the magnetic switching of the LSMO interlayer is abrupt and does not show any intermediate steps, while for LCMO a small intermediate step can be observed in some curves [see, e.g., Fig. 3(d)]. The latter may indicate the formation of two magnetic domains in the longer $\sim$700-nm LCMO junction, while the shorter $\sim$560-nm LSMO junction switches in a monodomain manner. This is in line with the expected size and geometry dependencies of domain configurations in ferromagnetic nanoparticles.

Altogether, the experimental data are consistent with the interpretation that the observed hysteretic MR loops of the junctions are due to a combination of ferromagnetic moment switching and CMR of the manganite barrier. The hysteresis arises from the finite coercive field for the remagnetization of the junction interlayer, while the CMR effect enables a resistive readout of the direction of magnetization. This facilitates a memory operation of the junction with just one F layer, as discussed below.

The simple linear MR (in a limited field range) allows us to reconstruct the *in situ* magnetization loop of the manganite nanoparticle forming the junction interlayer. The linear MR can be written as

$$R(H) = R(0) - \alpha|B(H)|, \tag{1}$$

where α is a constant coefficient, $R(0) = R(B = 0)$, and $B(H) = H + 4\pi M(H)$. For example, for $B > 0$, $|B| = H + 4\pi M$, and $R(H) = R(0) - \alpha H - 4\pi\alpha M(H)$. At high enough fields the ferromagnet is in the saturated magnetization state $M(H) = M_s$, which allows unambiguous determination of α from the slope of MR curves, $\alpha = |dR/dH|$ for $H > H_{\text{Coer}}$. Thus, $4\pi M(H) = (R(0) - R(H))/\alpha - H$. In general,

$$4\pi M = \pm \frac{R(0) - R(H)}{\alpha} - H, \tag{2}$$

where the sign corresponding to $|B|/B$ should be chosen.

Figures 5(a)–5(d) show magnetization loops that have been reconstructed from the MR loops in Figs. 3(d), 3(g),

4(c), and 4(e) for the LCMO [Figs. 5(a) and 5(b)] and the LSMO [Figs. 5(c) and 5(d)] interlayers [59]. Figures 5(a) and 5(c) show the loops at low T with superconducting YBCO electrodes, and Figs. 5(b) and 5(d) show the ones at $T = 100$ K for which YBCO is in the normal state [60]. The magnetization loops have a rectangular shape and exhibit an abrupt switching behavior between the saturated magnetization states. The overall behavior is typical for a monodomain switching along the easy axis, as expected for ferromagnetic nanoparticles with the applied field parallel to the longer side. This type of switching is sustained over a broad temperature range up to T_{Curie}. The persistence of this magnetic switching behavior to high temperature is also seen in Figures 5(e) and 5(f), which display temperature dependencies of the coercive fields H_{Coer} for the two junctions, deduced from the reconstructed magnetization loops. Apparently, manganite nanoparticles forming junction interlayers are acting as homogeneous (monodomain-type) CMR ferromagnets.

IV. MEMORY FUNCTIONALITY

The combination of ferromagnetism and colossal magnetoresistance provides a unique memory functionality in our junctions with just a single F layer. Figure 6 represents a sketch of the operation of such a CMR-based memory cell, which is based on the experimental MR loops of Fig. 3. The memory information is stored, as usual, in terms of the orientation of the magnetization of the interlayer ferromagnetic nanoparticle. For example, in Fig. 6 we interpret the states with the magnetization M pointing to the left and to the right as 1 and 0, respectively. The key requirement here is the switching of the ferromagnetic nanoparticle, which facilitates only two stable states with $M = \pm M_s$. This requirement is fulfilled in our junctions, as demonstrated in Fig. 5.

The resistance of the junction $R(B)$ is determined by the magnetic induction $B = H + 4\pi M$, according to Eq. (1). Without an applied field at $H = 0$, point A in Fig. 6, the two states are degenerate. This degeneracy is lifted if a local readout magnetic field H_{read} is applied, which should be smaller than the coercive field H_{Coer}. Due to the CMR phenomenon, the resistance R_1 of state 1, point B, with opposite directions of M and H_{read}, $R_1 = R(0) - 4\pi\alpha M_s + \alpha H_{\text{read}}$, is larger than the resistance R_0 of state 0, point C, with coaligned M and H, $R_0 = R(0) - 4\pi\alpha M_s - \alpha H_{\text{read}}$. The
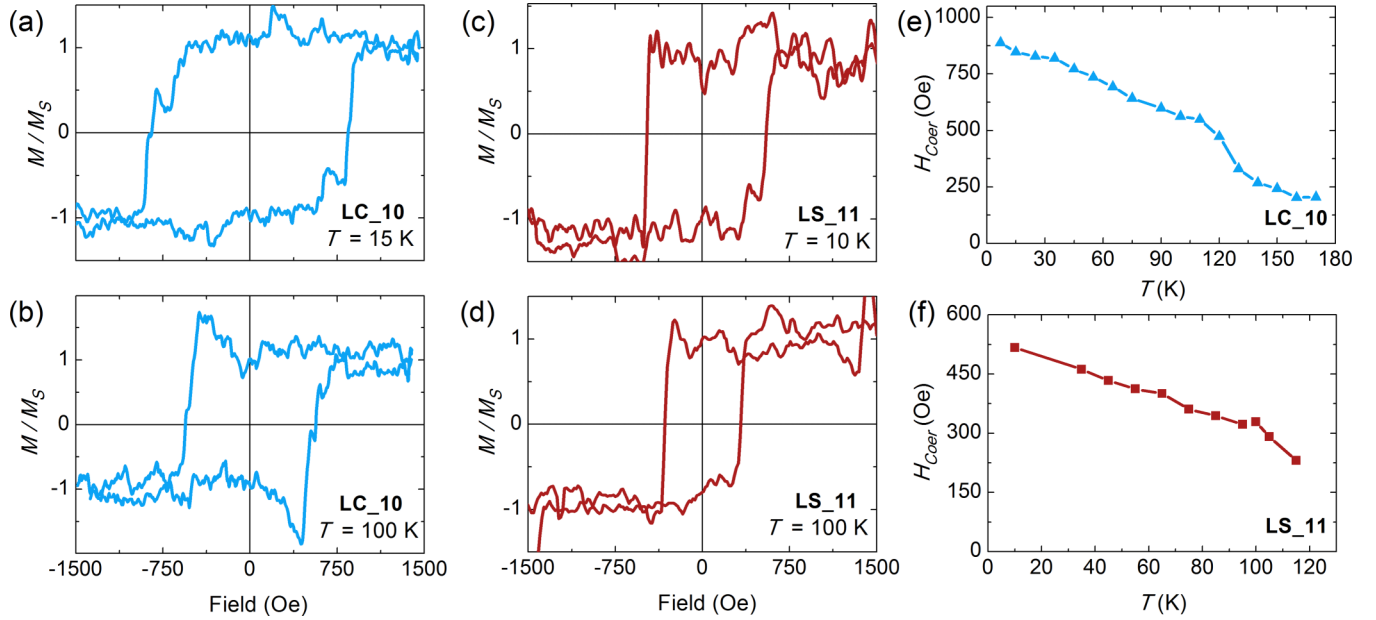
FIG. 5. Examples of magnetization loops reconstructed from the MR curves for the junction on YBCO/LCMO/YBCO (a) at 15 K and (b) at 100 K and for the junction on YBCO/LSMO/YBCO at (c) 10 K and (d) at 100 K. (e) and (f) Temperature dependence of $H_{Coer}(T)$ obtained from the hysteresis loops.

resistance change during the readout is $R_1 - R(A) = \alpha H_{read}$ or $R_0 - R(A) = -\alpha H_{read}$. A significant readout signal is facilitated here by the large CMR coefficient α. The readout signal can be doubled by sequential measurements at opposite readout fields, as marked by points B' and C' in Fig. 6. This increases the readout fidelity and reduces the required readout field.

For a multibit random-access memory application the readout field has to be local and individual for each cell to avoid cross talking. This may seem like a difficult task. However, instead of making a complex network of control lines, it is possible to utilize a self-field effect from the bias (readout) current for the generation of the local field at the junction. Such a self-field phenomenon is well known and often utilized in superconducting Josephson junctions [61,62]. Furthermore, the Meissner effect in superconductors leads to a so-called short-circuit principle in a system of current-carrying su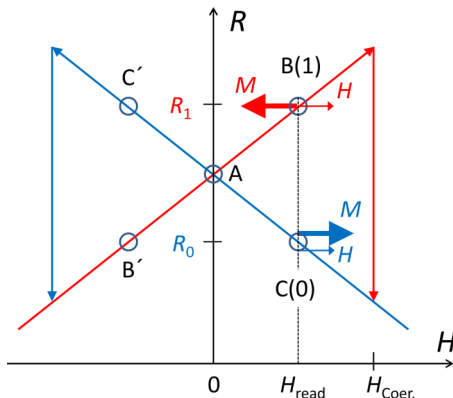perconducting electrodes. According to this principle, the current-induced magnetic field is localized and enhanced between electrodes and does not affect the surroundings, as if the electrodes were short-circuited. With a proper design of bias electrodes, this may greatly reduce the cross talking between neighboring memory cells.

Finally, we list the benefits of the proposed complex oxide YBCO/CMR-manganite/YBCO memory cells:

(i) The first is extreme simplicity. Only a single F-layer is required for the operation of the memory cell.

(ii) They are nonvolatile.

(iii) They have scalability to nanometer sizes. The manganites preserve their ferromagnetic properties down to a size of about ∼10 nm [55]. Such a miniaturization would require metallic manganites to reduce the junction resistance.

(iv) High-T_c superconductivity of YBCO allows comfortable operation at liquid-nitrogen temperature. Zero resistance of electrodes enables low power dissipation and high operation speed.

(v) The colossal magnetoresistance facilitates a large readout signal.

(vi) The CMR readout does not rely on superconductivity. Therefore, such a memory cell can be operated even at room temperature for manganites like LSMO with $T_{Curie} > 300$ K.

There are still many technical improvements needed before using such S/CMR/S devices as memory cells. The junction resistance should be decreased to reduce the switching energy. For this, doped metallic manganites should be used, which can carry supercurrent. The coercive field should also be reduced. This can be achieved by proper shape and geometry and doping and composition of the interlayer.

FIG. 6. Sketch of the operation principle of a bistable memory cell based on the CMR junctions.

V. CONCLUSIONS

To conclude, we fabricated complex oxide superconductor/ferromagnet/superconductor junctions with

layers of the high-T_c cuprate superconductor YBa$_2$Cu$_3$O$_{7-x}$ and the colossal magnetoresistive manganites La$_{2/3}$X$_{1/3}$MnO$_{3+\delta}$ (X=Ca or Sr). Nanoscale YBCO/LCMO/YBCO and YBCO/LSMO/YBCO junctions with a minimum feature size down to ∼275 nm were fabricated and studied experimentally. We found that the LCMO and LSMO layers of these junctions are qualitatively similar and behave as ferromagnetic insulators with Curie temperatures of about 210 K for LCMO and above 300 K for LSMO. Therefore, the junction characteristics, especially in the superconducting state of YBCO, carry solely information about the perpendicular transport properties of the manganite interlayers.

Our main experimental result is the observation of hysteretic magnetoresistance loops, which are caused by the CMR effect in the manganite interlayer and therefore persist both below and above the superconducting critical temperature $T_c \simeq 90$ K. The shape of the MR loops reflects the shape of ferromagnetic magnetization loops. This allows for an *in situ* reconstruction of the magnetization loops of the ferromagnetic nanoparticle that forms the junction interface. The magnetization loops have rectangular shapes with abrupt switching between the saturated magnetization states and are characteristic of a monodomain (or dual domain) switching of the ferromagnetic interlayer.

Finally, we have argued that the combination of a ferromagnetic response and a colossal magnetoresistance effect in our junctions facilitates memory functionality. In such a S-CMR-S memory cell the information is stored in the orientation of the magnetization of a single F layer, which can be read out at a finite magnetic field via the CMR effect.

The main benefits of such a memory cell are the extreme simplicity with only a single F layer; nonvolatility; scalability to nanometer sizes; high-T_c superconductivity of YBCO, which allows comfortable operation at liquid-nitrogen temperature, low power dissipation, and high operation speed; and the CMR facilitating large readout signals (or small readout fields). Furthermore, since the CMR readout does not rely on the unconventional proximity effect and triplet superconductivity in the F interlayer, such a memory cell can operate even at room temperature. We have argued that such a device can be one of the elements of complex oxide electronics in general and of a digital superconducting computer operating at liquid nitrogen in particular.

[1] A. I. Buzdin, Proximity effects in superconductor-ferromagnet heterostructures, Rev. Mod. Phys. **77**, 935 (2005).

[2] F. S. Bergeret, A. F. Volkov, and K. B. Efetov, Odd triplet superconductivity and related phenomena in superconductor-ferromagnet structures, Rev. Mod. Phys. **77**, 1321 (2005).

[3] Y. Asano, Y. Sawa, Y. Tanaka, and A. A. Golubov, Odd-frequency pairs and Josephson current through a strong ferromagnet, Phys. Rev. B **76**, 224525 (2007).

[4] M. Eschrig, Spin-polarized supercurrents for spintronics: A review of current progress, Rep. Prog. Phys. **78**, 104501 (2015).

[5] I. I. Soloviev, N. V. Klenov, S. V. Bakurskiy, M. Y. Kupriyanov, A. L. Gudkov, and A. S. Sidorenko, Beyond Moore's technologies: Operation principles of a superconductor alternative, Beilstein J. Nanotechnol. **8**, 2689 (2017).

[6] K. K. Likharev and V. K. Semenov, RSFQ logic/memory family: A new Josephson-junction technology for sub-terahertz-clock-frequency digital systems, IEEE Trans. Appl. Supercond. **1**, 3 (1991).

[7] O. A. Mukhanov, Energy-efficient single flux quantum technology, IEEE Trans. Appl. Supercond. **21**, 760 (2011).

[8] D. S. Holmes, A. L. Ripple, and M. A. Manheimer, Energy-efficient superconducting computing—Power budgets and requirements, IEEE Trans. Appl. Supercond. **23**, 1701610 (2013).

[9] T. Ortlepp and T. V. Duzer, Access time and power dissipation of a model 256-bit single flux quantum RAM, IEEE Trans. Appl. Supercond. **24**, 1 (2014).

[10] T. I. Larkin, V. V. Bol'ginov, V. S. Stolyarov, V. V. Ryazanov, I. V. Vernik, S. K. Tolpygo, and O. A. Mukhanov, Ferromagnetic Josephson switching device with high characteristic voltage, Appl. Phys. Lett. **100**, 222601 (2012).

[11] I. M. Dayton, T. Sage, E. C. Gingrich, M. G. Loving, T. F. Ambrose, N. P. Siwak, S. Keebaugh, C. Kirby, D. L. Miller, A. Y. Herr, Q. P. Herr, and O. Naaman, Experimental demonstration of a Josephson Magnetic Memory Cell with a programmable π-Junction IEEE Magn. Lett. **9**, 3301905 (2018).

[12] V. I. Zdravkov, D. Lenk, R. Morari, A. Ullrich, G. Obermeier, C. Müller, H.-A. Krug von Nidda, A. S. Sidorenko, S. Horn, R. Tidecks, and L. R. Tagirov, Memory effect and triplet pairing generation in the superconducting exchange biased Co/CoO$_x$/Cu$_{41}$Ni$_{59}$/Nb/Cu$_{41}$Ni$_{59}$ layered heterostructure, Appl. Phys. Lett. **103**, 062604 (2013).

[13] B. Baek, W. H. Rippard, S. P. Benz, S. E. Russek, and P. D. Dresselhaus, Hybrid superconducting-magnetic memory device using competing order parameters, Nat. Commun. **5**, 3888 (2014).

[14] I. P. Nevirkovets, O. Chernyashevskyy, G. V. Prokopenko, O. A. Mukhanov, and J. B. Ketterson, Superconducting-ferromagnetic transistor, IEEE Trans. Appl. Supercond. **24**, 1 (2014).

[15] T. Golod, A. Iovan, and V. M. Krasnov, Single Abrikosov vortices as quantized information bits, Nat. Commun. **6**, 8628 (2015).

[16] J. A. Glick, S. Edwards, D. Korucu, V. Aguilar, B. M. Niedzielski, R. Loloee, W. P. Pratt, N. O. Birge, P. G. Kotula, and N. Missert, Spin-triplet supercurrent in Josephson junctions containing a synthetic antiferromagnet with perpendicular magnetic anisotropy, Phys. Rev. B **96**, 224515 (2017).

[17] W. J. Gallagher and S. S. P. Parkin, Development of the magnetic tunnel junction MRAM at IBM: From first junctions to a 16-Mb MRAM demonstrator chip, IBM J. Res. Dev. **50**, 5 (2006).

[18] S. Bhatti, R. Sbiaa, A. Hirohata, H. Ohno, S. Fukami, and S. N. Piramanayagam, Spintronics based random access memory: A review, Mater. Today **20**, 530 (2017).

[19] J. W. A. Robinson, J. D. S. Witt, and M. G. Blamire, Controlled Injection of Spin-Triplet Supercurrents into a Strong Ferromagnet, Science **329**, 59 (2010).

[20] T. S. Khaire, M. A. Khasawneh, W. P. Pratt, and N. O. Birge, Observation of Spin-Triplet Superconductivity in Co-Based Josephson Junctions, Phys. Rev. Lett. **104**, 137002 (2010).

[21] A. Iovan, T. Golod, and V. M. Krasnov, Controllable generation of a spin-triplet supercurrent in a Josephson spin valve, Phys. Rev. B **90**, 134514 (2014).

[22] J. Linder and J. W. A. Robinson, Superconducting spintronics, Nat. Phys. **11**, 307 (2015).

[23] Y. Kalcheim, I. Felner, O. Millo, T. Kirzhner, G. Koren, A. Di Bernardo, M. Egilmez, M. G. Blamire, and J. W. A. Robinson, Magnetic field dependence of the proximity-induced triplet superconductivity at ferromagnet/superconductor interfaces, Phys. Rev B **89**, 180506(R) (2014).

[24] A. Iovan and V. M. Krasnov, Signatures of the spin-triplet current in a Josephson spin valve: A micromagnetic analysis, Phys. Rev. B **96**, 014511 (2017).

[25] R. S. Keizer, S. T. B. Goennenwein, T. M. Klapwijk, G. Miao, G. Xiao, and A. Gupta, A spin triplet supercurrent through the half-metallic ferromagnet CrO_2, Nature (London) **439**, 825 (2006).

[26] A. Singh, C. Jansen, K. Lahabi, and J. Aarts, High-Quality CrO_2 Nanowires for Dissipation-less Spintronics, Phys. Rev. X **6**, 041012 (2016).

[27] T. Hu, H. Xiao, C. Visani, Z. Sefrioui, J. Santamaría, and C. C. Almasan, Evidence from magnetoresistance measurements for an induced triplet superconducting state in $La_{0.7}Ca_{0.3}MnO_3/YBa_2Cu_3O_{7-\delta}$ multilayers, Phys. Rev. B **80**, 060506(R) (2009).

[28] K. Dybko, K. Werner-Malento, P. Aleshkevych, M. Wojcik, M. Sawicki, and P. Przyslupski, Possible spin-triplet superconducting phase in the $La_{0.7}Sr_{0.3}MnO_3/YBa_2Cu_3O_7/La_{0.7}Sr_{0.3}MnO_3$ trilayer, Phys. Rev. B **80**, 144504 (2009).

[29] Y. Kalcheim, T. Kirzhner, G. Koren, and O. Millo, Long-range proximity effect in $La_{2/3}Ca_{1/3}MnO_3/(100)YBa_2Cu_3O_{7-\delta}$ ferromagnet/superconductor bilayers: Evidence for induced triplet superconductivity in the ferromagnet, Phys. Rev. B **83**, 064510 (2011).

[30] C. Visani, Z. Sefrioui, J. Tornos, C. León, J. Briatico, M. Bibes, A. Barthélémy, J. Santamaría, and J. E. Villegas, Equal-spin Andreev reflection and long-range coherent transport in high-temperature superconductor/half-metallic ferromagnet junctions, Nat. Phys. **8**, 539 (2012).

[31] T. Golod, A. Rydh, V. M. Krasnov, I. Marozau, M. A. Uribe-Laverde, D. K. Satapathy, T. Wagner, and C. Bernhard, High bias anomaly in $YBa_2Cu_3O_{7-x}/LaMnO_{3+\delta}/YBa_2Cu_3O_{7-x}$ superconductor/ferromagnetic insulator/superconductor junctions: Evidence for a long-range superconducting proximity effect through the conduction band of a ferromagnetic insulator, Phys. Rev. B **87**, 134520 (2013).

[32] I. Marozau, P. T. Das, M. Döbeli, J. G. Storey, M. A. Uribe-Laverde, S. Das, C. Wang, M. Rössle, and C. Bernhard, Influence of La and Mn vacancies on the electronic and magnetic properties of $LaMnO_3$ thin films grown by pulsed laser deposition, Phys. Rev. B **89**, 174422 (2014).

[33] J. Chakhalian, J. W. Freeland, A. J. Millis, C. Panagopoulos, and J. M. Rondinelli, Colloquium: Emergent properties in plane view: Strong correlations at oxide interfaces, Rev. Mod. Phys. **86**, 1189 (2014).

[34] M. Imada, A. Fujimori, and Y. Tokura, Metal-insulator transitions, Rev. Mod. Phys. **70**, 1039 (1998).

[35] E. Dagotto, When oxides meet face to face, Science **318**, 1076 (2007).

[36] J. G. Bednorz and K. A. Müller, Possible high Tc superconductivity in the Ba-La-Cu-O system, Z. Phys. B **64**, 189 (1986).

[37] R. von Helmolt, J. Wecker, B. Holzapfel, L. Schultz, and K. Samwer, Giant Negative Magnetoresistance in Perovskitelike $La_{2/3}Ba_{1/3}MnO_x$ Ferromagnetic Films, Phys. Rev. Lett. **71**, 2331 (1993).

[38] Th. Jacobs, Y. Simsek, Y. Koval, P. Müller, and V. M. Krasnov, Sequence of Quantum Phase Transitions in $Bi_2Sr_2CaCu_2O_{8+\delta}$ Cuprates Revealed by *in situ* Electrical Doping of One and the Same Sample, Phys. Rev. Lett. **116**, 067001 (2016).

[39] H. M. Christen and G. Eres, Recent advances in pulsed-laser deposition of complex oxides, J. Phys.: Condens. Matter **20**, 264005 (2008).

[40] H. Y. Hwang, Y. Iwasa, M. Kawasaki, B. Keimer, N. Nagaosa, and Y. Tokura, Emergent phenomena at oxide interfaces, Nat. Mater. **11**, 103 (2012).

[41] M. Bibes, J. E. Villegas, and A. Barthélémy, Ultrathin oxide films and interfaces for electronics and spintronics, Adv. Phys. **60**, 5 (2011).

[42] G. E. Eperon, T. Leijtens, K. A. Bush, R. Prasanna, T. Green, J. T.-W. Wang, D. P. McMeekin, G. Volonakis, R. L. Milot, R. May, A. Palmstrom, D. J. Slotcavage, R. A. Belisle, J. B. Patel *et al.*, Perovskite-perovskite tandem photovoltaics with optimized band gaps, Science **354**, 861 (2016).

[43] D. Zhao, Y. Yu, C. Wang, W. Liao, N. Shrestha, C. R. Grice, A. J. Cimaroli, L. Guan, R. J. Ellingson, K. Zhu, X. Zhao, R.-G. Xiong, and Y. Yan, Low-bandgap mixed tin-lead iodide perovskite absorbers with long carrier lifetimes for all-perovskite tandem solar cells, Nat. Energy **2**, 17018 (2017).

[44] H. Kim, J. S. Han, S. G. Kim, S. Y. Kim, and H. W. Jang, Halide perovskites for resistive random-access memories, J. Mater. Chem. C **7**, 5226 (2019).

[45] F. S. Galasso, *Perovskites and high-Tc superconductors* (Gordon and Breach, New York, 1990).

[46] H.-U. Habermeier and G. Cristiani, Cuprate/Ferromagnetic Oxide Superlattices, J. Supercond. **15**, 425 (2002).

[47] Z. Sefrioui, D. Arias, V. Peña, J. E. Villegas, M. Varela, P. Prieto, C. León, J. L. Martínez, and J. Santamaría, Ferromagnetic/superconducting proximity effect in $La_{0.7}Ca_{0.3}MnO_3/YBa_2Cu_3O_{7-\delta}$ superlattices, Phys. Rev. B **67**, 214511 (2003).

[48] V. K. Malik, I. Marozau, S. Das, B. Doggett, D. K. Satapathy, M. A. Uribe-Laverde, N. Biškup, M. Varela, C. W. Schneider, C. Marcelot, J. Stahn, and C. Bernhard, Pulsed laser deposition growth of heteroepitaxial $YBa_2Cu_3O_7/La_{0.67}Ca_{0.33}MnO_3$ superlattices on $NdGaO_3$ and $Sr_{0.7}La_{0.3}Al_{0.65}Ta_{0.35}O_3$ substrates, Phys. Rev. B **85**, 054514 (2012).

[49] A. M. Goldman, P. I. Kraus, K. Nikolaev, V. Vas'ko, A. Bhattacharya, and W. Cooley, Spin Injection and Transport in Magnetic-Superconducting Oxide Heterostructures, J. Supercond. **14**, 283 (2001).

[50] P. Przyslupski, S. Kolesnik, E. Dynowska, T. Skoskiewicz, and M. Sawicki, Fabrication and Properties of $YBa_2Cu_3O_7/RE_{1-x}A_xMnO_{3-y}$ multilayers, IEEE Trans. Appl. Supercond. **7**, 2192 (1997).

[51] G. A. Ovsyannikov, Y. V. Kislinskii, K. Y. Constantinian, A. V. Shadrin, V. V. Demidov, and A. M. Petrzhik, Spin-filter tunneling in superconducting mesa structures with a ferromagnetic manganite interlayer, J. Exp. Theor. Phys. **124**, 628 (2017).

[52] L. Righi, P. Gorria, M. Insausti, J. Gutiérrez, and J. M. Barandiarán, Influence of Fe in giant magnetoresistance ratio and magnetic properties of $La_{0.7}Ca_{0.3}Mn_{1-x}Fe_xO_3$ perovskite type compounds, J. Appl. Phys. **81**, 5767 (1997).

[53] A. Urushibara, Y. Moritomo, T. Arima, A. Asamitsu, G. Kido, and Y. Tokura, Insulator-metal transition and giant magnetoresistance in $La_{1-x}Sr_xMnO_3$, Phys. Rev. B **51**, 14103 (1995).

[54] Note that a small shoulder appears in $R(T)$ curves of the bridge after the first cut [Fig. 1(f)]. It can be caused for two reasons: The first is partial penetration of current into the manganite interlayer due to a finite voltage in the bridge (which is still in the resistive state). The junction area does show slightly reduced T_c [see Figs. 2(b) and 2(c)], which may be due to either the proximity effect or interface mixing. The second is the

[55] R. de Andrés Prada, T. Golod, C. Bernhard, and V. M. Krasnov, Growth and nanofabrication of all-perovskite superconducting/ferromagnetic/superconducting junctions, J. Supercond. Novel Magn., 1 (2019), doi: 10.1007/s10948-019-5023-6.

[56] J. Chakhalian, J. W. Freeland, H.-U. Habermeier, G. Cristiani, G. Khaliullin, M. van Veenendaal, and B. Keimer, Orbital Reconstruction and Covalent Bonding at an Oxide Interface, Science **318**, 1114 (2007).

[57] T. Holden, H.-U. Habermeier, G. Cristiani, A. Golnik, A. Boris, A. Pimenov, J. Humlíček, O. I. Lebedev, G. Van Tendeloo, B. Keimer, and C. Bernhard, Proximity induced metal-insulator transition in $YBa_2Cu_3O_7/La_{2/3}Ca_{1/3}MnO_3$ superlattices, Phys. Rev. B **69**, 064505 (2004).

[58] M. Flokstra, J. M. van der Knaap, and J. Aarts, Magnetic coupling in superconducting spin valves with strong ferromagnets, Phys. Rev. B **82**, 184523 (2010).

[59] The magnetization curve in the Fig. 5(c) data is obtained from the $R(H)$ data in Fig. 4(c). Although the $R(H)$ curve looks noisy, the distortion is mostly a vertical offset, which is removed by appropriate subtraction, providing the corresponding cleaner $M(H)$ curve in Fig. 5(c).

[60] The magnetization curve in Fig. 5(b) exhibits a dip just before switching. Most likely, this is an artifact of a linear-fit subtraction, presumably due to a nonlinearity of magnetoresistance at this T [see Fig. 3(b)].

[61] V. M. Krasnov, V. A. Oboznov, and N. F. Pedersen, Fluxon dynamics in long Josephson junctions in the presence of a temperature gradient or spatial nonuniformity, Phys. Rev. B **55**, 14486 (1997).

[62] T. Golod, O. M. Kapran, and V. M. Krasnov, Planar Superconductor-Ferromagnet-Superconductor Josephson Junctions as Scanning-Probe Sensors, Phys. Rev. Appl. **11**, 014062 (2019).

formation of a weak link in the YBCO electrode in the region of the cut.